LETTERS

Polarons and confinement of electronic motion to two dimensions in a layered manganite

H. M. Rønnow[1], Ch. Renner[2], G. Aeppli[2], T. Kimura[3] & Y. Tokura[4]

A remarkable feature of layered transition-metal oxides—most famously, the high-temperature superconductors—is that they can display hugely anisotropic electrical and optical properties (for example, seeming to be insulating perpendicular to the layers and metallic within them), even when prepared as bulk three-dimensional single crystals. This is the phenomenon of 'confinement', a concept at odds with the conventional theory of solids, and recognized[1] as due to magnetic and electron–lattice interactions within the layers that must be overcome at a substantial energy cost if electrons are to be transferred between layers. The associated energy gap, or 'pseudogap', is particularly obvious in experiments where charge is moved perpendicular to the planes, most notably scanning tunnelling microscopy[2] and polarized infrared spectroscopy[3]. Here, using the same experimental tools, we show that there is a second family of transition-metal oxides—the layered manganites $La_{2-2x}Sr_{1+2x}Mn_2O_7$—with even more extreme confinement and pseudogap effects. The data demonstrate quantitatively that because the charge carriers are attached to polarons (lattice- and spin-textures within the planes), it is as difficult to remove them from the planes through vacuum-tunnelling into a conventional metallic tip, as it is for them to move between Mn-rich layers within the material itself.

The manganese perovskite oxides (manganites) have been the subject of a decade-long revival, spurred by the colossal magnetoresistance[4,5] of thin films and sustained by the large variety of physical phenomena—including Jahn-Teller distortions, charge, spin and orbital ordering[6–9]—manifested in carefully prepared single crystals. A fruitful new area has been the layered manganites, the most prominent of which is $La_{2-2x}Sr_{1+2x}Mn_2O_7$ (LSMO). They are built from perovskite bilayers as found in the pseudocubic parent compound (La,Sr)MnO_3, separated by rock-salt-type lanthanide and alkaline-earth ion oxide sheets in a tetragonal crystal structure (Fig. 1a). These materials can be viewed as self-assembled stacks of two-dimensional electronic liquids weakly coupled to each other. They display the same anisotropic electric resistance (Fig. 1b) as the high-temperature superconductors (HTSs), and the same tunnelling magnetoresistance as top-down fabricated spintronic devices, where switching from the low- to the high-resistance state occurs via conversion from antiparallel to parallel configurations of the spins in adjacent bilayers[10].

The lamellar structure of some HTS copper oxides has been very advantageous for experiments that are traditionally suitable for surface science, namely photoemission and scanning tunnelling microscopy (STM). Much less information of this type is available for the manganites, especially their layered polymorphs. Here we report atomic scale microscopy and temperature-dependent spectroscopy of unprecedentedly large and (for manganites) flat surfaces of LSMO, providing definitive evidence for confinement but finding no evidence—in this particular oxide—for the popular concept of electronic phase separation[11] where different electronic states coexist in adjacent regions.

As a function of Sr doping x, LSMO exhibits the familiar features of many manganites[12]. On cooling from the high-temperature paramagnetic state, LSMO develops a charge-ordered insulator around $x = 0.5$ and a variety of ferro- and antiferromagnetic phases between $x = 0.45$ and $x = 0.30$. We investigate the $x = 0.30$ compound,

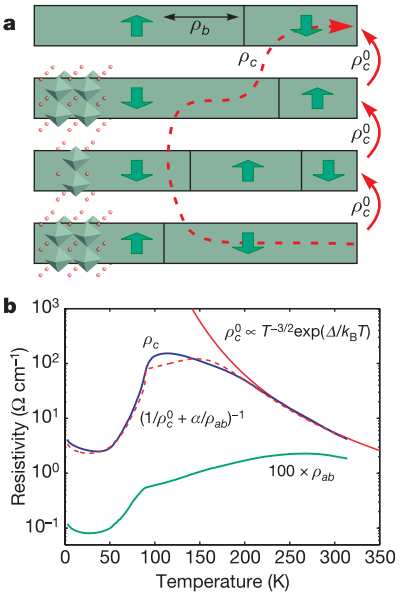

Figure 1 | Structure and bulk transport properties of $La_{1.4}Sr_{1.6}Mn_2O_7$. **a**, Bilayer perovskite structure and different paths considered for the *c*-axis transport. Green arrows depict the ferromagnetic domains, and the dashed red line a possible reduced-resistance *c*-axis conduction path. **b**, The measured in-plane resistivity, ρ_{ab} (green), and *c*-axis resistivity, ρ_c (blue), drop dramatically below the ferromagnetic ordering temperature. The high-temperature part of the *c*-axis resistivity fits a purely activated behaviour (red), $\rho_c^0(T) \propto T^{-3/2}\exp(\Delta_\rho/2k_BT)$, with $\Delta_\rho = 188$ meV. The dashed red line depicts a model that includes in-plane contributions through conductivity enhancements at magnetic stacking faults. It places the intrinsic *c*-axis resistance $\rho_c^0(T)$ in parallel with a shunt resistance that is the product of $\rho_{ab}(T)$ and a prefactor $\alpha^{-1}(T)$, determined by the distances that the carriers travel within the planes, as well as the probability of moving carriers between parallel magnetized bilayers in the defective regions where adjacent bilayers have parallel magnetizations. Because the latter quantity grows with the magnetic order parameter M appearing below T_c, we use the Ansatz that $\alpha(T) = aM^2(T) + b$.

[1]Laboratory for Neutron Scattering, ETH-Zürich and Paul Scherrer Institut, 5232 Villigen, Switzerland. [2]London Centre for Nanotechnology & Department of Physics and Astronomy, University College London, Gower Street, London WC1E 6BT, UK. [3]Bell Laboratories, Lucent Technologies, 600 Mountain Avenue, Murray Hill, New Jersey 07974, USA. [4]Department of Applied Physics, University of Tokyo, Bunkyo-ku, Tokyo 113-8656, Japan, and Spin Superstructure Project (SSS), ERATO, Japan Science and Technology Agency (JST), Tsukuba 305-0046, Japan.

whose outstanding feature, shared with optimally and underdoped HTSs, is that in the paramagnetic phase the electrical resistance within the planes appears metallic—decreasing with decreasing temperature—while that corresponding to hopping between them is much larger and insulating (Fig. 1b). Below $T_c = 90$ K, the material orders as an antiferromagnetic stack of two-dimensional ferromagnets (the bilayers), and the electrical properties in zero field track each other, following the paradigm of dirty metals with quantum corrections[13].

We performed STM using tungsten tips in ultrahigh vacuum at temperatures from 5 to 400 K. *In situ* cleavage at room temperature of the LSMO single crystals[14] produced clean and extremely flat surfaces (peak-to-peak roughness below 0.3 Å over micrometre-sized terraces, Fig. 2a). As three-dimensional perovskites like $LaMnO_3$ do not cleave, LSMO must break between the perovskite bilayers, in agreement with the observed steps that are half a unit cell high (Fig. 2a). Yet, despite the smooth surfaces, atomic resolution remains elusive, except for tiny islands containing approximately 30 unit cells with the expected 3.86 Å Mn ion spacing lattice parameter (Fig. 2b), and slightly raised (above the background terrace) by an amount too small to be ascribed to adsorbed impurities. The low density of small and stable (reproducible over many hours, Fig. 2c–e) islands should not be regarded as phase separation, but as a local perturbation by some atomic-scale defect in the otherwise homogeneous system.

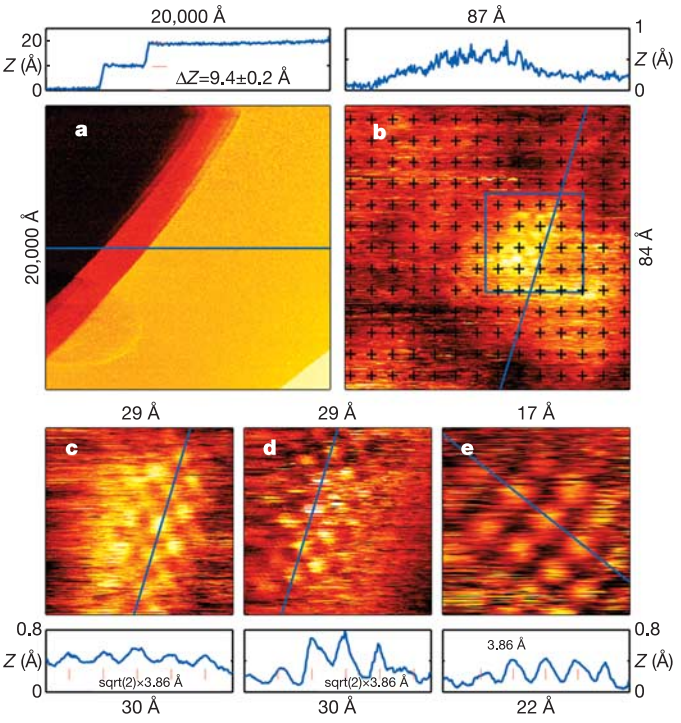

Figure 2 | Unprocessed STM micrographs of $La_{1.4}Sr_{1.6}Mn_2O_7$. The sample is held at a positive potential relative to the STM tip ($V = 0.8$ V, $I = 0.2$ nA), implying that we are primarily probing the unoccupied electronic density of states of the manganite. **a**, *In situ* cleaving exposed atomically flat micrometre-sized terraces (imaged at 212 K). On this scale, the nonlinear response of the piezoelectric STM scanner accounts for the curved appearance of the steps. Nominal scan amplitudes are given next to each panel. **b**, **c**, Higher-magnification images of the same cluster obtained in separate runs. Atomic-scale resolution is always restricted to tiny regions, containing about 30 unit cells (imaged at 283 K). Crosses in **b** indicate the positions (±3 Å) where a subset of the spectra averaged in Fig. 3b was measured. **d**, **e**, Two other instances of tiny regions with atomic resolution at 283 K. The amplitude profiles show selected cross-sections from each micrograph ($Z(X,Y)$, blue lines), highlighting the half-unit-cell high steps (**a**) and the systematically enhanced tunnelling conductance (**b**) associated with atomic-scale resolution of the in-plane 3.86 Å unit-cell (**c**–**e**).

Spatially resolved tunnelling spectroscopy can establish electronic phase separation into metallic and insulating regions[15,16] and determine whether there is a specific signature associated with the magnetic metal–insulator transition at $T_c = 90$ K. Therefore, for each temperature, we measured and analysed thousands of current–voltage characteristics, $I(V)$, at different locations over areas ranging from 10 to 10^6 nm^2. Several conclusions can be directly read from the representative data in Fig. 3a, b. First, the current distribution (white band) for each bias stemming from 2,000 spectra exactly matches the spread in each individual spectrum (dots), meaning that the spectra are extremely homogeneous over micrometre-sized regions at all temperatures. Furthermore, at 283 K, the regions with resolved atoms are spectroscopically indistinguishable (to within current experimental error) from surrounding featureless areas. Our most remarkable discovery is also directly visible in Fig. 3: the spectrum is gapped at 44 K (that is, essentially no current flows between two bias voltages, V_+ and V_-), seemingly at odds with the bulk transport measurements[17] showing a two orders of magnitude drop in resistivity to metallic behaviour below 90 K.

To quantify the tunnelling characteristics, we evaluate the zero-bias conductance, σ_0, namely the slopes of $I(V)$ at $V = 0$ (red line in Fig. 3a, b). For each temperature, the slopes from thousands of spectra fall on a normal distribution, gradually shifting away from zero on increasing the temperature (Fig. 3c, inset). The increase of spread with temperature is a purely instrumental effect, accounted for by a constant electronic noise enhanced by the temperature dependence of the STM's piezoelectric coefficients. Hence, at no temperature do our data show any sign of electronic phase separation into metallic and insulating regions, which would yield two peaks

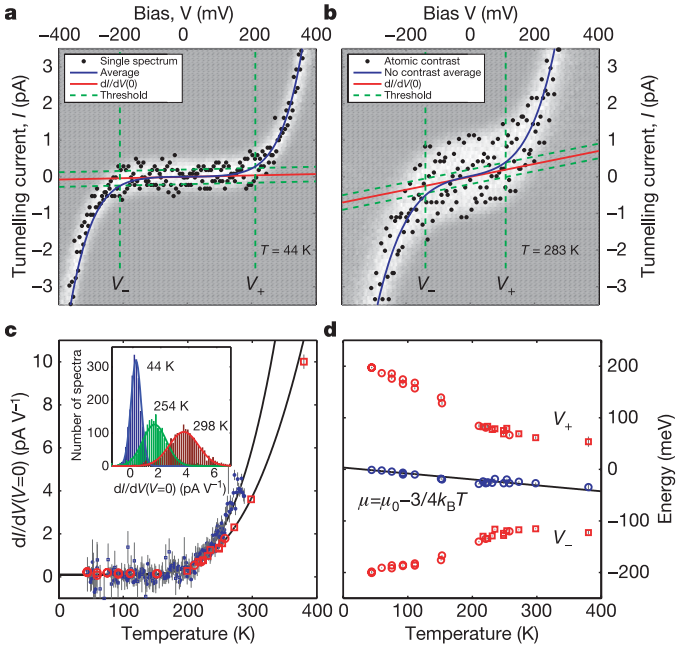

Figure 3 | Temperature-dependent STM spectroscopy of $La_{1.4}Sr_{1.6}Mn_2O_7$. **a**, **b**, $I(V)$ at 44 K (**a**) and at 283 K (**b**); a subset of sampling positions are indicated in Fig. 2b (see text for further details). **c**, Tunnelling conductance σ_0 at $V = 0$ as a function of temperature. The open symbols are obtained from the averages of thousands of $I(V)$ spectra measured over large areas at fixed temperatures. Filled symbols derive from single $I(V)$ characteristics measured on slowly warming. Fitting $\sigma_0(T)$ to $T^{3/2}\exp(-\Delta/2k_BT)$ gives $\Delta = 196 \pm 12$ meV for both sets of data. The inset shows the uniform distribution of σ_0 obtained from thousands of $I(V)$ characteristics measured at individual points on large areas at selected fixed temperatures. **d**, Temperature dependence of the gap edges V_- and V_+, showing the persistence of the gap below the metal–insulator transition at 90 K. Blue circles indicate the mid-gap energy $(V_+ + V_-)/2$, which is independent of the chosen threshold (0.2 pA in this case) and corresponds to the chemical potential μ.

rather than the observed single peak in the distribution of σ_0 values.

The temperature (T) dependence of $\sigma_0(T) \propto T^{3/2} \exp(-\Delta/2k_BT)$, where k_B is Boltzmann's constant, is consistent with a thermally activated conductance across a gap $\Delta = 196 \pm 12$ meV at the Fermi energy (Fig. 3c), in agreement with the gap $\Delta_\rho = 188$ meV found from fitting the high-temperature c-axis resistivity (ρ_c) to the thermally activated form (Fig. 1b). Because the detailed nature of the tunnel junction changes between experiments, the absolute value of the zero-bias slope may vary (Fig. 3c). However, it does not affect the extracted gap, giving additional confidence that we are probing a gap intrinsic to LSMO.

Whereas σ_0 can be determined in a robust manner, it is more difficult to extract Δ from the tunnelling spectra. Bearing in mind that the zero-bias slope is simply due to thermal activation, we define V_- (V_+) as the negative (positive) bias at which the tunnelling current departs by a given amount (threshold) from the ohmic background (Fig. 3d). The gap amplitude, defined as $\Delta = V_+ - V_-$, depends on the particular choice of threshold, but its dramatic temperature dependence, doubling between room and base temperatures, much less so. Surprisingly, a more conventional linear behaviour is found for the chemical potential, $\mu = (V_+ + V_-)/2 \approx -3/4k_BT$, which, assuming the classic law $\mu = -3/4k_BT \ln(m_e/m_h)$ for an intrinsic semiconductor[18], yields $m_e/m_h = 2.7$, implying that holes travel more easily along the c axis than electrons. (Here m_h (m_e) is the hole (electron) effective mass.)

Optical reflectivity is another probe of the electronic excitation spectra of solids, and has the advantages of much less surface sensitivity than photoemission and scanning tunnelling spectroscopy (STS), in addition to not depending on the details—crucial for d.c. conductivity—of electrical current flow in a macroscopic sample with electrical contacts. Consistency between optical data and STS is therefore a definitive demonstration of whether the STS measurements represent surface or intrinsic bulk phenomena. Accordingly, Fig. 4 shows the optical conductivity[19] for LSMO. When polarized photons drive the carriers to move within the planes, the low-energy part of the spectra displays a marked Drude-like tail below T_c, signalling metallic behaviour (Fig. 4a) in excellent agreement with the in-plane resistivity data of Fig. 1b. In contrast, there is no sign of a metallic Drude-like peak in the c-axis optical conductivity (Fig. 4b), which shows a clear gap with no spectral weight up to about 400–500 meV (except for sharp phonon bands in the range 20–80 meV). The conductivity onset energy is entirely consistent with the low-temperature gap $\Delta = V_+ - V_-$ deduced from our STS spectra.

What is striking about our findings is the consistency of the STS and c-axis optical conductivity. Furthermore, the same gap value characterizes the temperature-dependent spectroscopy and the high temperature ρ_c, indicating that both measurements probe the same bulk property. However, on cooling we uncover the curious result that STS seems oblivious to the Néel point (90 K), below which ρ_c displays seemingly metallic behaviour while the zero-bias conductance, the STS spectra and $\sigma_c(\omega)$ are all consistent with an insulator (here ω is frequency). How can we reconcile the striking discrepancy below T_c between macroscopic resistivity measurements and the vacuum tunnelling and optical spectroscopies? The most obvious idea is to assert, as has been done on the basis of analysis of X-ray data for samples exposed to air, that the surface probed via tunnelling is somehow insulating and non-magnetic[20], and therefore different from the bulk sampled in electrical measurements. However, this is at odds with spin-polarized scanning electron microscopy clearly demonstrating that the top layer is ferromagnetic[21], the in-plane metallic screening (see ref. 22 and discussion below) underlying the general lack of atomic contrast in ultrahigh-vacuum STM, static secondary ion mass spectroscopy suggesting that the top 1 nm of our cleaved sample has the same chemical composition as the bulk, and the agreement of STS and the much less surface-sensitive optical conductivity results.

The data show that whatever dominates the d.c. conductivity along c has no effect on the optical and STS measurements. To account for the d.c. metallicity, we consider LSMO as a stack of alternating metallic and insulating layers. In a perfect sample, the c-axis transport would always be thermally activated, with ρ_c diverging at low temperature in agreement with the STM experiments. The sudden drop of ρ_c at the ferromagnetic transition must then be due to a parallel conduction mechanism. The idea is that while adjacent bilayers have predominantly antiparallel magnetizations, there will be defects where the domain walls in adjacent layers do not exactly coincide, resulting in regions containing adjacent bilayers whose magnetizations are parallel (Fig. 1a). In these regions the tunnelling probability will be enhanced, as demonstrated by the large and negative c-axis magnetoresistance seen in the low-temperature limit[10,12]. Whereas the defective regions only contribute weakly to ρ_c above T_c, they turn into a well-connected network below T_c, effectively shunting the cation layers. Indeed, as depicted in Fig. 1b, $\rho_c(T)$ is reproduced by a simple model, described in the legend, with the activated intrinsic c-axis resistance $\rho_c^0(T) \propto T^{-3/2} \exp(\Delta_\rho/2k_BT)$ in parallel with the shunt resistance dominated by $\rho_{ab}(T)$ (where ρ_{ab} is the in-plane resistivity). As $\rho_c^0(T)$ diverges on lowering the temperature, the intrinsic anisotropy becomes larger and the c-axis resistance increasingly mimics the in-plane resistivity. In contrast, the parallel channel is inoperative in the STM tunnelling process, where a vacuum barrier is maintained between the tip and the sample surface, and so does not contribute to the temperature-dependent zero-bias conductance.

The key findings of our investigations are (1) position-independent and (2) gapped tunnelling and c-axis optical spectra at all temperatures, (3) metallic in-plane optical and d.c. conductivity, (4) c-axis d.c. conductivity that follows an activated form consistent with both STS and $\sigma_c(\omega)$ at high T but then tracks the in-plane d.c. conductivity rather than the STS zero-bias conductance at low T, and (5) atomic resolution that is stable and reproducible but limited to very small regions on the extremely flat surfaces prepared in ultrahigh

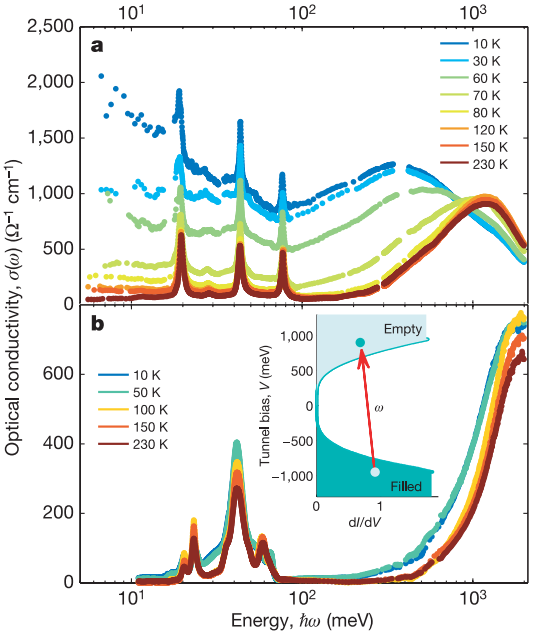

Figure 4 | Optical conductivity deduced from near-normal-incidence reflectivity measured on single crystal samples (sharp peaks at 20–80 meV are due to phonons)[19]. **a**, In-plane optical conductivity. The dramatic increase at low frequencies (ω) below 90 K corresponds to Drude-like metallic behaviour. **b**, The c-axis optical conductivity shows a semiconductor-like absorption edge at around 4–500 meV. Inset shows how the conductivity is related to a filled to empty state transition in the single particle density of states measured via STM (Fig. 3a, b). Imperfect alignment of the photon polarization and the crystal c-axis mixes the measured in-plane and out-of-plane conductivities, and is the most likely cause of the leftward shift of the absorption edge on cooling.

vacuum. All indications from the STM data themselves—including the step heights and lattice parameters measured when atomic resolution is found—demonstrate that the results are intrinsic to cleaved surfaces of LSMO. Furthermore, we have presented detailed evidence and analysis indicating that the STS, optical and d.c. conductivity measurements are entirely consistent with each other. This leaves us with the challenge of understanding the underlying anisotropy in quasiparticle transport out of the planes in LSMO and the surprising observation (5).

The quasiparticles in strongly correlated materials can be very different and more complex than the renormalized electrons found in simple metals. As STS extracts or inserts single (bare) electrons, the quasiparticles must dissociate in the tunnelling process. Even if the quasiparticles form a metal in the plane, STS will measure a gap corresponding to the energy it takes to destroy the quasiparticle to extract the electron (hole) from the MnO layer. Thus, when the transport, STS and optical data on LSMO are taken together, we are left with a picture where charge carriers are confined to metallic bilayers in LSMO, and cannot escape without a finite energy transfer. This is true down to the lowest temperatures, where our LSMO samples are magnetically ordered, and the conventional theory of solids would suggest a fully three-dimensional metal. The charge carriers are therefore bound to larger objects that can move within, but not between, the planes. Possible candidates for such objects are the polarons whose effects on the lattice and spin texture have been seen using X-rays and neutron scattering[23,24]. Polarons have also been associated with the pseudogap observed by angle-resolved photoemission spectroscopy (ARPES)[25] in LSMO with $x = 0.4$ and the gap measured by STM[26] in the pseudo-cubic compound $La_{1-x}Ca_xMnO_3$ with $x = 0$ and $x = 0.3$. Most recently, detailed ARPES experiments led to a very similar description of LSMO ($x = 0.4$) in terms of a polaronic metal with a gapped anisotropic electronic structure[27].

It turns out that the same polaron picture provides a similarly clear understanding of observation (5), and is at the heart of our discovery of atomic-scale features in a metallic manganite. Specifically, the general inability to resolve atoms—in contrast to the case for the charge-ordered manganite (Bi,Ca)MnO_3 (ref. 28)—suggests metallic screening of charges within the *a*–*b* planes, in agreement with the bulk in-plane conductivity data. Typically, STM can only image metal atoms (for example, in gold) under conditions where there is bonding and relative motion between the tip and sample atoms. For the parameters achievable in our measurements, screening would reduce atomic contrast to below 0.02 Å (ref. 22). The small areas where atomic resolution is attained must therefore be regions where screening is relieved, owing perhaps to a point defect.

In some famous experiments[29] on much simpler metals, and recently on HTSs[30], quasiparticle scattering at defects results in electron density modulations with periodicities fixed by the quasiparticle dispersion relation. Obviously a sufficiently strong defect may bind (trap) a quasiparticle, resulting in a static (non-dispersive) STM pattern reflecting the internal structure of the polaron. There is some experimental evidence for this phenomenon in the copper oxides[31] at energies below the quasiparticle dispersion effects. Here, we speculate that this is what is occurring when we see atoms in LSMO, and our experiments may have captured the real-space image of that very elusive object—a trapped polaron. The trapped polaron concept could account not only for the relative paucity of regions with resolved atoms on surfaces that were optimized for smoothness and cleanliness, but would also explain their common size, which in fact coincides with neutron and X-ray scattering results[23,24] for the lattice and spin textures associated with polarons.

Received 6 September 2005; accepted 13 February 2006.

1. Anderson, P. W. The resonating valence bond state in La_2CuO_4 and superconductivity. *Science* **235,** 1196–1198 (1987).
2. Renner, Ch., Revaz, B., Genoud, J. Y., Kadowaki, K. & Fischer, Ø. Pseudogap precursor of the superconducting gap in under- and overdoped $Bi_2Sr_2CaCu_2O_{8+\delta}$. *Phys. Rev. Lett.* **80,** 149–152 (1998).
3. Uchida, S., Tamasaku, K. & Tajima, S. c-axis optical spectra and charge dynamics in $La_{2-x}Sr_xCuO_4$. *Phys. Rev. B* **53,** 14558–14574 (1996).
4. von Helmolt, R., Wecker, J., Holzapfel, B., Schultz, L. & Samwer, K. Giant negative magnetoresistance in perovskitelike $La_{2/3}Ba_{1/3}MnO_x$ ferromagnetic films. *Phys. Rev. Lett.* **71,** 2331–2333 (1993).
5. Jin, S. *et al.* Thousandfold change in resistivity in magnetoresistive La-Ca-Mn-O films. *Science* **264,** 413–415 (1994).
6. Millis, A. J. Lattice effects in magnetoresistive manganese perovskites. *Nature* **392,** 147–150 (1998).
7. Ramirez, A. P. *et al.* Thermodynamic and electron diffraction signatures of charge and spin ordering in $La_{1-x}Ca_xMnO_3$. *Phys. Rev. Lett.* **76,** 3188–3191 (1996).
8. Mori, S., Chen, C. H. & Cheong, S.-W. Pairing of charge-ordered stripes in (La,Ca)MnO_3. *Nature* **392,** 473–476 (1998).
9. Tokura, Y. & Nagaosa, N. Orbital physics in transition-metal oxides. *Science* **288,** 462–468 (2000).
10. Perring, T. G., Aeppli, G., Kimura, T., Tokura, Y. & Adams, M. A. Ordered stack of spin valves in a layered magnetoresistive perovskite. *Phys. Rev. B* **58,** R14693–R14696 (1998).
11. Dagotto, E. in *Nanoscale Phase Separation and Colossal Magnetoresistance* (eds Cardona, M. *et al.*) (Springer Series in Solid State Sciences Vol. 136, Springer, New York, 2003).
12. Kimura, T. & Tokura, Y. Layered magnetic manganites. *Annu. Rev. Mater. Sci.* **30,** 451–474 (2000).
13. Abrikosov, A. A. Quantum interference effects in quasi-two-dimensional metals. *Phys. Rev. B* **61,** 7770–7774 (2000).
14. Moritomo, Y., Asamitsu, A., Kuwahara, H. & Tokura, Y. Giant magnetoresistance of manganese oxides with a layered perovskite structure. *Nature* **380,** 141–144 (1996).
15. Becker, T. *et al.* Intrinsic inhomogeneities in manganite thin films investigated with scanning tunneling spectroscopy. *Phys. Rev. Lett.* **89,** 237203 (2002).
16. Fäth, M. *et al.* Spatially inhomogeneous metal-insulator transition in doped manganites. *Science* **285,** 1540–1542 (1999).
17. Kimura, T. *et al.* Interplane tunneling magnetoresistance in a layered manganite crystal. *Science* **274,** 1698–1701 (1996).
18. Kittel, C. *Introduction to Solid State Physics* (Wiley and Sons, Inc., New York, 1976).
19. Ishikawa, T., Tobe, K., Kimura, T., Katsufuji, T. & Tokura, Y. Optical study on the doping and temperature dependence of the anisotropic electronic structure in bilayered manganites: $La_{2-2x}Sr_{1+2x}Mn_2O_7$ ($0.3 \leq x \leq 0.5$). *Phys. Rev. B* **62,** 12354–12362 (2000).
20. Freeland, J. W. *et al.* Full bulk spin polarization and intrinsic tunnel barriers at the surface of layered manganites. *Nature Mater.* **4,** 62–67 (2005).
21. Konoto, M. *et al.* Direct imaging of temperature-dependent layered antiferromagnetism of a magnetic oxide. *Phys. Rev. Lett.* **93,** 107201 (2004).
22. Blanco, J. M. *et al.* First-principles simulations of STM images: From tunneling to the contact regime. *Phys. Rev. B* **70,** 085405 (2004).
23. Perring, T. G., Aeppli, G., Moritomo, Y. & Tokura, Y. Antiferromagnetic short-range order in a two dimensional manganite exhibiting giant magnetoresistance. *Phys. Rev. Lett.* **78,** 3197–3200 (1997).
24. Campbell, B. J. *et al.* Structure of nanoscale polaron correlations in $La_{1.2}Sr_{1.8}Mn_2O_7$. *Phys. Rev. B* **65,** 014427 (2001).
25. Dessau, D. S. *et al. k*-dependent electronic structure, a large "ghost" Fermi surface, and a pseudogap in a layered magnetoresistive oxide. *Phys. Rev. Lett.* **81,** 192–195 (1998).
26. Wei, J. Y. T., Yeh, N. C. & Vasquez, R. P. Tunneling evidence of half-metallic ferromagnetism in $La_{0.7}Ca_{0.3}MnO_3$. *Phys. Rev. Lett.* **79,** 5150–5153 (1997).
27. Mannella, N. *et al.* Nodal quasiparticle in pseudogapped colossal magnetoresistive manganites. *Nature* **438,** 474–478 (2005).
28. Renner, Ch., Aeppli, G., Kim, B. G., Soh, Y. A. & Cheong, S.-W. Atomic-scale images of charge ordering in a mixed-valence manganite. *Nature* **416,** 518–521 (2002).
29. Crommie, M. F., Lutz, C. P. & Eigler, D. M. Imaging standing waves in a two-dimensional electron gas. *Nature* **363,** 524–527 (1993).
30. Hoffman, J. E. *et al.* Imaging quasiparticle interference in $Bi_2Sr_2CaCu_2O_{8+\delta}$. *Science* **297,** 1148–1151 (2002).
31. Yazdani, A., Howald, C. M., Lutz, C. P., Kapitulnik, A. & Eigler, D. M. Impurity-induced bound excitations on the surface of $Bi_2Sr_2CaCu_2O_8$. *Phys. Rev. Lett.* **83,** 176–179 (1999).

Acknowledgements We thank T. Ishikawa for providing the optical conductivity data shown in Fig. 4, D. McPhail and R. Chater for the static SIMS measurements, and A. Fisher and J. Mesot for discussions. We acknowledge support from a Wolfson-Royal Society Research Merit Award, the NEC corporation, and the European Commission through a FW6 STREP programme. H.M.R. thanks T. F. Rosenbaum for support through an NSF Materials Research Science and Engineering Centers grant.

Author Information Reprints and permissions information is available at npg.nature.com/reprintsandpermissions. The authors declare no competing financial interests. Correspondence and requests for materials should be addressed to Ch.R. (c.renner@ucl.ac.uk).